IEEE Access
Multidisciplinary | Rapid Review | Open Access Journal

Received September 10, 2019, accepted September 23, 2019, date of publication October 4, 2019, date of current version October 16, 2019.

Digital Object Identifier 10.1109/ACCESS.2019.2945556

Micro-Vessel Image Segmentation Based on the AD-UNet Model

ZHONGMING LUO[1], YU ZHANG[1], LEI ZHOU[1], BINGE ZHANG[2], JIANAN LUO[1], AND HAIBIN WU[1]

[1]The Higher Education Key Laboratory for Measuring and Control Technology and Instrumentations of Heilongjiang Province, National Experimental Teaching Demonstration Center of Measuring and Control Technology, Harbin University of Science and Technology, Harbin 150080, China
[2]Heilongjiang Institute of Construction Technology, Harbin 150025, China

Corresponding author: Zhongming Luo (luozhongming@hrbust.edu.cn)

This work was supported in part by the National Natural Science Foundation of China under Grant 61671190, and in part by the Project of Heilongjiang Education Department in China under Grant 12541140.

ABSTRACT Retinal vessel segmentation plays a vital role in computer-aided diagnosis and treatment of retinal diseases. Considering the low contrast between retinal vessels and the background image, complex structural information as well as blurred boundaries between tissue and blood vessels, the retinal vessel image segmentation algorithm based on the improved U-Net network is proposed in the paper. The algorithm introduces an attention mechanism and densely connected network into the original U-Net network and realizes the automatic segmentation of retinal vessels. According to the test results of the algorithm on commonly-used datasets of the DRIVE and STARE fundus images, respectively, the accuracy is 0.9663 and 0.9684; the sensitivity is 0.8075 and 0.8437; the specificity is 0.9814 and 0.9762; the AUC values are 0.9846 and 0.9765; and the F-measures are 0.8203 and 0.8419, respectively. In the paper, the Attention-Dense-UNet (AD-UNet) algorithm is applied to segment human bulbar conjunctival micro-vessels. The experimental results show that the algorithm can achieve ideal segmentation results.

INDEX TERMS Image segmentation, attention mechanism, densely connected network, micro-vessels.

I. INTRODUCTION

Retinal vasculopathy of the human body can reflect the severity of cardiovascular diseases such as hypertension, coronary heart disease and diabetes. The screening of the morphological characteristics and number of retinal blood vessels can assist doctors in diagnosing patients' conditions. Therefore, the accuracy of retinal vessel segmentation is quite important. In clinical practice, retinal vessel segmentation is usually performed by manual segmentation, which is influenced by human factors, requires additional time, and cannot meet the requirements of large-scale fundus image processing. Therefore, finding an efficient and accurate fundus image segmentation algorithm through computer assistance to realize automatic segmentation technology for vessel images is significant for improving the diagnosis efficiency of vessel diseases and reducing medical costs.

So far, domestic and foreign researchers have proposed numerous effective vessel segmentation methods, which can be roughly divided into unsupervised learning and supervised learning. Unsupervised learning includes the matching filter method, fuzzy clustering method, edge detection method and morphological method. Giri *et al.* [1] proposed an automatic segmentation method for retinal vessel images. The method enhances image contrast by matching filtering and obtains segmentation results by spatially weighted fuzzy C-mean clustering. Usman *et al.* [2] enhanced blood vessels with two-dimensional Gabor wavelet and sharpening filter, and positioned and segmented blood vessels through an edge detection algorithm and morphological operation. Wang *et al.* [3] proposed a fundus image segmentation method with multi-scale 2D Gabor wavelet transform, extracted coarse and fine blood vessels with different respective methods, and found that the final segmentation result was the union of the two. Liang *et al.* [4] proposed a retinal vessel segmentation algorithm combining regional energy fitting information and a level set shape prior model.

Supervised learning segments vessel images mainly through feature learning by deep learning. Oliveira *et al.* [5] segmented the vessel images using wavelet transform

The associate editor coordinating the review of this manuscript and approving it for publication was Md. Asikuzzaman.

and a multi-scale convolutional neural network and effectively solved the complex structure of retinal vessels. Diego *et al.* [6] classified pixels through a neural network whose training features are 7-D vectors composed of pixels based on gray level and moment invariants. Liskowski and Krawiec [7] conducted vessel segmentation with a deep neural network model. Jiang *et al.* [8] proposed a multi-scale convolutional neural network. The model can obtain more dense feature information and better capture retinal vessel information of different sizes. Dharmawan *et al.* [24] put forward a new hybrid vessel segmentation algorithm based on the U-Net network. Ren *et al.* [25] conducted vessel segmentation with a support vector machine (SVM) classifier. Unsupervised learning has high segmentation speed and a simple algorithm but usually results in lower segmentation results than the supervised learning algorithm.

Considering the low contrast between retinal vessels and the background image, complex structural information as well as blurred boundaries between tissue and blood vessels, an AD-UNet blood vessel segmentation method is proposed in this paper. First, the method decreases the image noise and enhances the contrast of the blood vessels and the background through preprocessing operations on color fundus images. It then improves the original U-Net network of retinal vessel image segmentation by adding an attention mechanism and densely connected network, making full use of the characteristic information of each layer and more effectively solves problems such as gradient diffusion through the densely connected network. In addition, the introduction of the attention mechanism, achieves better positioning of the fundus area of interest, thus improving the efficiency of the algorithm. The experimental results show that the algorithm can solve the problem of insufficient segmentation of tiny thin vessels.

The rest of this article is organized as follows. We describe the micro-vessel image preprocessing and AD-UNet model in Section II. Section III introduces the image datasets and the evaluation metrics. We then discuss and compare our experimental results from many aspects. Finally, a conclusion is drawn in Section IV.

II. RETINAL MICRO-VESSEL IMAGE SEGMENTATION

A. IMAGE PREPROCESSING

Due to the influence of uneven illumination on the sites of retinal micro-vessels in the image acquisition process, as well as the low contrast of the vessel images in the target area and background, along with blurry blood vessels and organizational boundaries, problems such as fracture may appear in blood vessel segmentation. Therefore, it is necessary to conduct the fundus image enhancements during preprocessing and to better highlight the contrast between the blood vessels and the background. Retinal images are RGB color images that are broken into red, green and blue monochrome channels for analysis. According to Fig. 1 (b), (c) and (d), the green channel has higher contrast between the blood vessels and the background and lower noise interference, while the red and

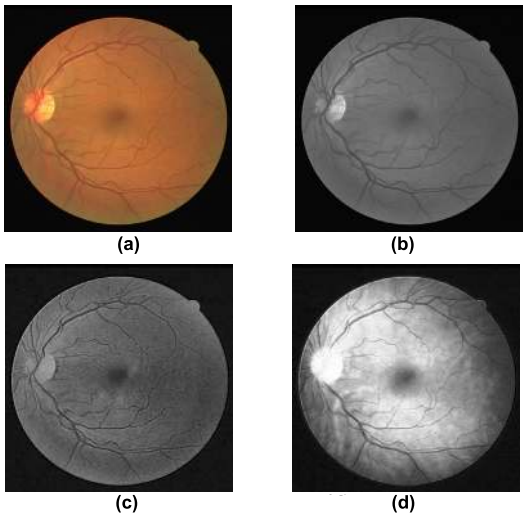

FIGURE 1. Retinal R, G and B channel images. (a) DRIVE dataset fundus image, (b) G channel image, (c) B channel image, (d) R channel image.

FIGURE 2. CLAHE image.

blue channels have lower contrast between the blood vessels and the background and higher noise interference. Despite the overall red tone of fundus images, the computational analysis of the RGB channel following image grayscale conversion finds small pixel value differences between the red channel vessels and the background, which is detrimental to the vessel segmentation. Moreover, part of the vessel information is lost due to the highlighting in the optic disc region. In contrast, pixel value differences between the green channel vessels and the background are rather large and thus conducive to vessel segmentation. Therefore, this paper adopts the green channel of fundus images for processing.

Aiming at the retinal micro-vessel green channel image, the method of limiting contrast histogram equalization (CLAHE) is adopted for enhancement processing. The CLAHE method can effectively overcome noise and better highlight the contrast between different local blood vessels and the background. Fig. 2 shows the retinal vessel image enhanced by the CLAHE method.

In the paper, the fundus images in the DRIVE and STARE datasets are adjusted to 512*512 in size and converted into grayscale images in order to balance the size of the original image and reduce the complexity of the model. The grayscale image is normalized, with the expression as follows:

$$I = \frac{I - \mu}{\sigma} \tag{1}$$

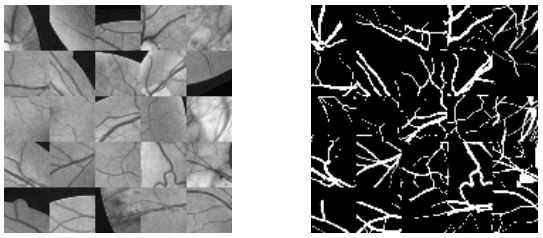

FIGURE 3. Examples of patches and corresponding labels for images from the DRIVE dataset. (a) Image patches; (b) Corresponding ground truth.

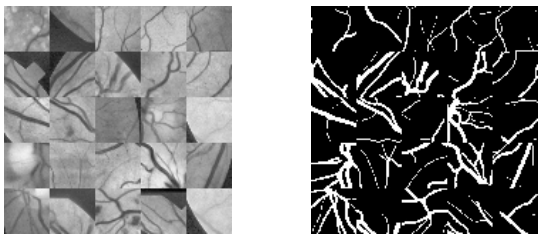

FIGURE 4. Examples of patches and corresponding labels for images from the STARE dataset. (a) Image patches; (b) Corresponding ground truth.

where μ and σ respectively represent the mean and standard deviation of grayscale image I.

There are too few images in the DRIVE and STARE datasets. To effectively avoid the overfitting phenomenon in the training process of the model, the data are enhanced by rotating and clipping the preprocessed training images. In the paper, the sliding window size is 96*96; the local areas of ground truth and training images are randomly cut to extract block target information. Such a method is conducive to obtaining contour features of blood vessels and enables the network model to obtain more useful feature information form fundus images. Examples of patches and corresponding labels for images from the DRIVE dataset and STARE dataset are shown in Fig. 3 and Fig. 4.

B. AD-UNet MODEL

1) U-Net MODEL

Convolutional neural networks(CNN) learn useful feature information from low-level features, and then discard the low-level feature information, which leads to inefficient utilization of feature information and serious degradstion of learning ability of the model. Thus, it appears to be particularly important to enhance the feature information reutilization by the network model. Inspired by the U-Net network [9], [26] and [29] and densely connected network [10] and [28], this paper proposes an AD-UNet model for vessel segmentation purposes. Fig. 5 displays the overall framework of the model. The AD-UNet network structure proposed herein is divided into three components, namely, the encoder, the decoder and the attention mechanism, of which the encoder and decoder components are added with dense blocks. The sizes of convolution kernels in the network are all set to 3×3, and the vessel and background areas are segmented using the SoftMax activation function. The conventional U-Net network is introduced into dense connections to enhance the transmission efficiency of features and enrich the feature information extracted by the network, thereby preferably solving the loss of fine vessel details and improving the accuracy of network segmentation.

2) DENSENET MODEL

The CNN only connects the output feature map of the l^{th} layer as input to the $(l+1)^{th}$ layer, which is defined as: $x_l = H_l(x_{l-1})$. To improve the efficiency of feature utilization, this paper introduces a densely connected network to enable efficient reutilization of network features, which substantially reduces the number of network parameters, suppresses the overfitting of small datasets and mitigates the vanishing gradient phenomenon. Setting the output of network layer l as x_l, the output definition of the lth layer of the model is as follows:

$$x_l = H_l([x_o, x_1, \cdots, x_{l-1}]) \tag{2}$$

where $[x_o, x_1, \cdots, x_{l-1}]$ denotes the union of feature graph output by the $0, 1, \cdots, l-1$ layer. In the paper, the U-Net model and DenseNet are combined to construct a single Dense Block network structure, as shown in Fig. 6.

In Fig. 6, BN is batch normalization. DenseNet, through full use of the characteristic information of each layer, shortens the training time, addresses the loss of fine vessel details, and improves the accuracy of vessel segmentation.

3) ATTENTION MECHANISM

Attention mechanism [11], a model first proposed by Bahdanau *et al.* [12], can simulate human brain attention, and it has been applied in the field of machine translation. This mechanism has the ability to focus on the input features and can screen the features of interest from a huge amount of feature information. It can be seen from the retinal vessel segmentation results in reference [27] that problems such as inaccurate positioning of the ROI by the algorithm and inclusion of fundus contour information in segmentation results caused degradation of vessel segmentation accuracy. In this paper, the attention mechanism is introduced into our proposed model in order to avoid similar problems in the segmentation results. In view of the complex problem of locating the region of interest (ROI) in the fundus images, which is affected by the diversity of fundus diseases and image noise interference, the ROI of fundus images and the background areas in the DRIVE and STARE datasets are used in the paper. The ROI has a pixel value of 1, while the background area has a pixel value of 0. The model only focuses on the target ROI. By applying the attention mechanism to the fundus contour features, it effectively avoids interference from background information, enables better location of fundus areas of interest, and improves the efficiency of the algorithm. In the AD-UNet model of the paper, the penultimate feature graph and the product of the attention mask are used to implement the

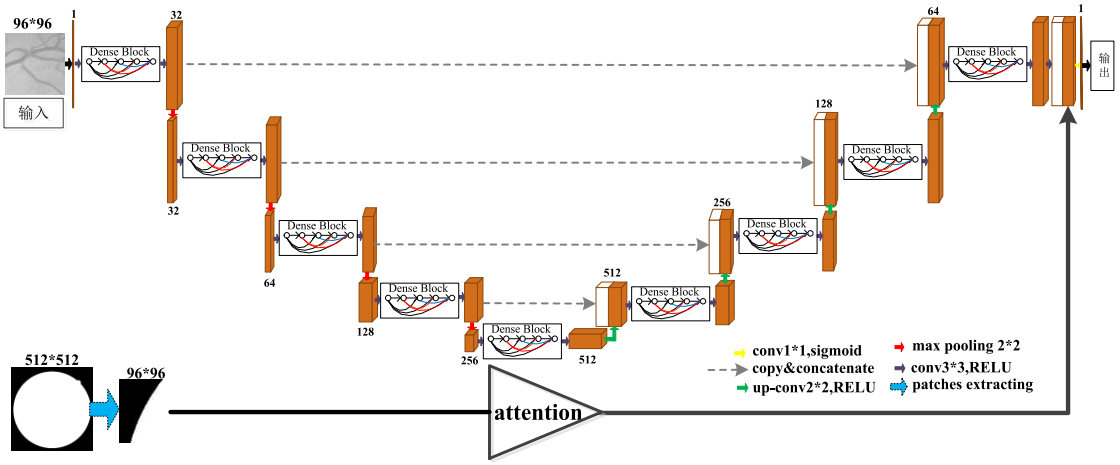

FIGURE 5. The architecture of the AD-UNet.

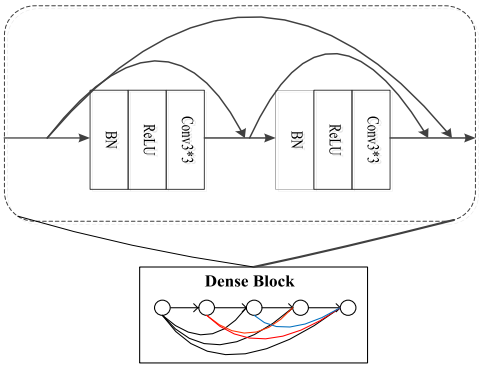

FIGURE 6. Dense block.

attention mechanism, the expression of which is as follows:

$$I(x,y) = \begin{cases} A(x,y)^*1 & (x,y) \in ROI \\ A(x,y)^*0 & (x,y) \notin ROI \end{cases} \quad (3)$$

where $A(x, y)$ represents the features at the location of (x, y).

4) LOSS FUNCTION

Only 10% of pixels in the fundus image are blood vessels, indicating a large proportional gap between vessel and background pixels. If the characteristics of fundus images are not fully taken into account in the designed loss function, it is more inclined to segment the background region during the model learning process. Wang *et al.* [27] trained the vessel segmentation model using the dice coefficient loss function, which might result in training instability. Therefore, in the AD-UNet network, the error rate of pixel segmentation is minimized by cross validation, the loss function is optimized by the Adam algorithm, and the learning rate is 0.001. The cross entropy loss function is defined as follows:

$$J_{CE}(y,\hat{y}) = -\frac{1}{n}\sum_{n} y_i log\hat{y}_i + (1-y_i)log(1-\hat{y}_i) \quad (4)$$

where y_i denotes the ground truth and $\hat{y}_i$ represents the forecast data.

III. EXPERIMENTS AND ANALYSIS

A. EXPERIMENTAL ENVIRONMENT AND DATASET

Pycharm is used as the software environment of the experiment. In addition, Keras and TensorFlow neural network libraries are used. The hardware platform is the Intel(R)Core(TM) i5-3232m CPU@2.60GHz, 8GB memory, and the Nvidia GeForce GT740M GPU.

The retinal vessel images used in the paper are international public databases, namely, the DRIVE (Digital Retinal Images for Vessel Extraction) database [13] and the STARE (Structured Analysis of the Retina) database [14]. The DRIVE database is randomly selected from 400 diabetic patients in the Netherlands and includes 40 RGB color images, 20 training data and 20 test data. The size of the images is 565*584, and each fundus image has the standard segmentation map manually marked by experts, which is called the ground truth image. The STARE database is provided by the University of California, San Diego. It contains 20 fundus images (10 images with lesions and 10 images without lesions). The images are in convenient bitmap PPM format, the image size is 700*605, each color channel in the image is 8-bit, and each image is manually labeled by two experts according to the ground truth.

B. COMPARISON OF VESSEL SEGMENTATION RESULTS OF DIFFERENT ALGORITHMS

In the paper, the effectiveness of the AD-UNet segmentation algorithm is verified with the DRIVE and STARE datasets and compared with the segmentation results in [23], [19] and [22], as shown in Fig.7. The first includes and the second one are the pathological fundus images from the DRIVE dataset; the third includes the healthy fundus images from the DRIVE dataset, and the fourth and fifth are the fundus images from the STARE dataset. Fig. 7 (a) is the original image; Fig. 7 (b) is the ground truth; Fig. 7 (c) is the result according to the algorithm in the paper; Fig. 7(d) is the segmentation result of the generative adversarial network (V-GAN); Fig. 7 (e) is the segmentation result of

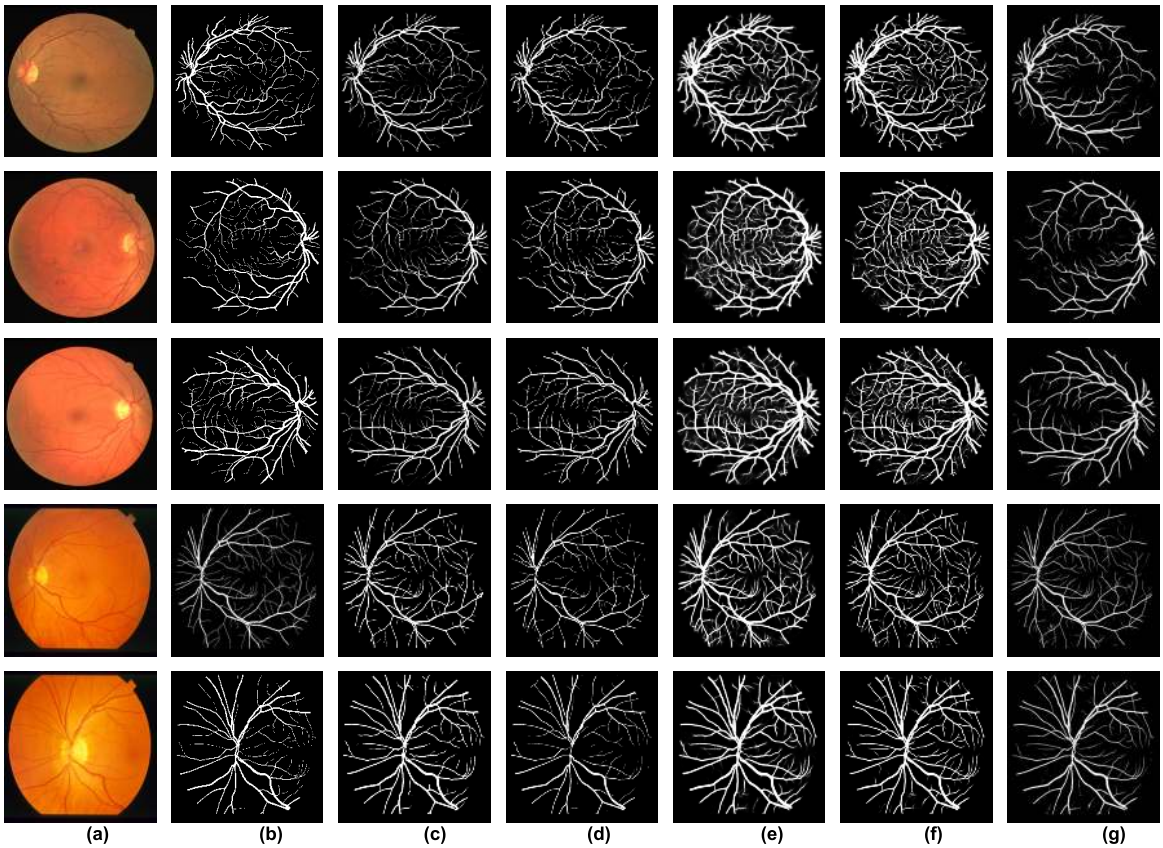

FIGURE 7. Results of fundus image segmentation by different algorithms. (a) Original image, (b) Ground truth, (c) AD-UNet algorithm, (d) V-GAN algorithm, (e) HED algorithm, (f) DRIU algorithm, (g) U-Net algorithm.

holistically-nested edge detection (HED); Fig. 7 (f) is the segmentation result of deep retinal image understanding (DRIU); and Fig. 7 (g) is the segmentation result of U-Net.

As observed for the first and second fundus images in Fig. 7, for the images of fundus with lesions analyzed by the algorithm proposed in the paper, tiny and coarse blood vessels show better segmentation performance and stronger robustness in terms of segmentation results than the ground truth for complex areas of cross blood vessels and low contrast tiny blood vessels.By contrast,the V-GAN algorithm is affected by lesions: a fracture phenomenon appears in the vessel segmentation results, and more micro-vessel details are lost. Moreover, retinal optic disc regions segmented by the HED algorithm and DRIU algorithm contain more noise information, and the blood vessels segmented by these algorithms are relatively thick. For the U-Net algorithm, there is a fracture phenomenon, and tiny blood vessels have poorer segmentation performance at the ends of the vessel branches. Based on the vessel segmentation results of the third fundus image, the algorithm proposed in the paper, V-GAN algorithm and DRIU algorithm segment more micro-vessel information and show better segmentation results for tiny vessels, while the HED algorithm cannot segment tiny vessels clearly and the blood vessels are relatively thick compared with the ground truth image. The vessel size result produced by the U-Net algorithm is nearly consistent with the ground truth, but more tiny blood vessels are lost at the ends of the vessel branches. According to the fourth and fifth pieces of fundus image blood vessel segmentation results, the algorithm proposed in the paper can show accurate segmentation results for the retinal optic disc region, and segmented blood vessels will not break. Therefore, the introduced DenseNet and attention mechanism in the algorithm can effectively access the complex feature information of fundus images. By comparison, as for the V-GAN algorithm, there is a fracture phenomenon in the main blood vessel segmentation of the retinal optic disc region, the blood vessel details are lost, and tiny blood vessels have poorer segmentation performance at the ends of the vessel branches. There is an undersegmentation problem for the HED and DRIU algorithms, which yield coarser segmentation of blood vessels. There is an over-segmentation problem for the U-Net algorithm and segmented blood vessels will break. In conclusion, the segmentation of fundus images by the algorithm in the paper exhibits better performance for the segmentation of tiny blood vessels, including reduced noise and stronger robustness.

C. DETAILED COMPARISON OF VESSEL SEGMENTATION RESULTS BY DIFFERENT ALGORITHMS

In order to more clearly highlight the advantages of the algorithm in the paper for segmentation of fundus images, the detailed information comparison of vessel segmentation

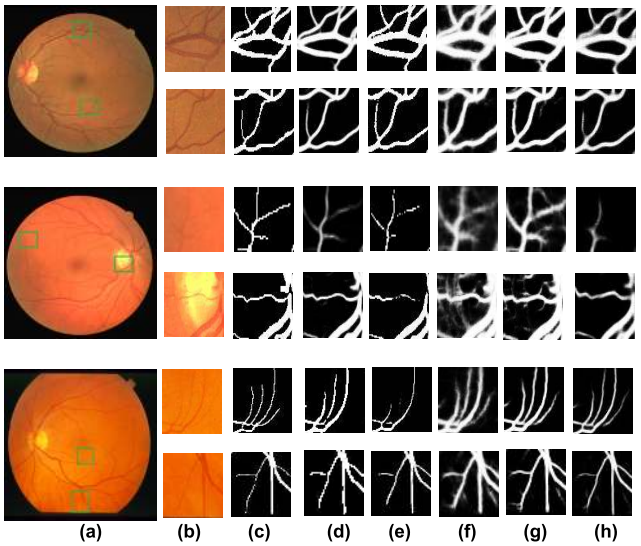

FIGURE 8. Comparison of fundus image segmentation performance by different algorithms. (a) Original image, (b)Local region of original image, (c) Ground truth, (d) AD-UNet algorithm, (e) V-GAN algorithm, (f) HED algorithm, (g) DRIU algorithm, (h) U-Net algorithm.

in the DRIVE and STARE datasets with the V-GAN algorithm, HED algorithm, DRIU algorithm and U-Net algorithm is shown in Fig. 8. Fig. 8 illustrates local images of retinal vessel intersections, optic disc areas, and branch ends. Fig. 8(a) and 8 (b) are the original image and the local region of the original image, respectively; Fig. 8(c) is the ground truth of the corresponding locally enlarged image; Fig. 8(d), Fig. 8(e), Fig. 8(f), Fig. 8(g) and Fig. 8 (h) are the local regional image segmentation results of the algorithm in the paper, V-GAN algorithm, HED algorithm, DRIU algorithm and U-Net algorithm, respectively. Fundus image blood vessels have complex structures: the tiny blood vessels at the ends of branches cannot be recognized by human eyes and the optic disc areas have high brightness, so the contrast between blood vessels and background area is reduced, making it difficult to accurately segment the detailed information of blood vessels. In vessel cross areas, the HED algorithm also can detect the edge information for small receptive field edge points, and it, therefore, segments coarser blood vessels than the ground truth under the influence of the network; there is an obvious sawtooth phenomenon for the V-GAN algorithm segmentation results. The DRIU algorithm can accurately segment the blood vessel details, proving the network model is ability to capture the information of vessel characteristics. The segmentation results of the U-Net algorithm are ambiguous when segmenting closer blood vessel areas. In the paper, DenseNet is added to the original U-Net network and the attention mechanism is introduced so as to make full use of the characteristic information of each layer and to capture the vessel details to the maximum extent. Therefore, the phenomenon of vessel fracture is effectively avoided when segmenting the vessel crossing area. In the area of the fundus optic disc, the V-GAN algorithm presents the problem of vessel fracture, and the segmentation results of the HED algorithm and DRIU algorithm are ambiguous and exhibit undersegmentation. However, the segmentation results of the U-Net algorithm and the algorithm in the paper are roughly the same as the ground truth, and the segmented blood vessels are relatively smooth and reasonable. In the end areas of the vessel branches, the V-GAN algorithm has limitations and a vessel rupture problem; the HED algorithm results present undersegmentation and unclear blood vessels; the DRIU algorithm segmentation results are roughly consistent with the ground truth, reflecting the stronger ability of the network to the vessel detail information acquisition. The vessel size results obtained by the U-Net algorithm are almost consistent with the ground truth, but some segmentation results present over-segmentation and under-segmentation. Furthermore, the results produced by the algorithm proposed in the paper are almost consistent with the ground truth, and the sizes of the blood vessels are not changed.

According to the experimental results, the method of improving the original U-Net segmentation results by introducing DenseNet and the attention mechanism can segment different regions of blood vessels and obtains better segmentation results than other algorithms. Therefore, the superiority of this algorithm in the segmentation of complex fundus vessel structures is fully reflected.

D. PERFORMANCE COMPARISON OF DIFFERENT SEGMENTATION ALGORITHMS

In order to evaluate the algorithm in this paper more accurately, the algorithm in this paper is compared with the methods in the references on unsupervised learning methods [15]–[17], [3], [4] and the references on supervised learning methods [18]–[22] in the DRIVE and STARE dataset, respectively. Indicators such as the sensitivity, specificity, accuracy and F-measure are adopted as measurement standards. The expressions are as follows:

$$Sensitivity = \frac{T_P}{T_P + F_N} \tag{5}$$

$$Specificity = \frac{T_N}{T_N + F_P} \tag{6}$$

$$Accuracy = \frac{T_N + T_P}{T_P + T_N + F_P + F_N} \tag{7}$$

$$TPR = \frac{T_P}{T_P + F_N} \tag{8}$$

$$FPR = \frac{F_P}{F_P + T_N} \tag{9}$$

$$Precision = \frac{T_P}{T_P + F_P} \tag{10}$$

$$Recall = \frac{T_P}{T_P + F_N} \tag{11}$$

$$F - measure = 2 \times Precision \times \frac{Recall}{Precision + Recall} \tag{12}$$

where T_P, T_N, F_P and F_N represent true positive, true negative, false positive and false negative, respectively. Sensitivity indicates the percentage of correctly classified vessel pixels

TABLE 1. Retinal vessel segmentation results of the DRIVE dataset.

Type	Method	Acc(%)	Sen(%)	Spe(%)	AUC	F-measure
Unsupervised methods	Mendonca[15]	0.9450	0.7340	0.9760	0.8550	—
	Soomro[16]	0.9430	0.7530	0.9760	0.9691	—
	Khan[17]	0.9510	0.7340	0.9670	—	—
	Wang[3]	0.9457	0.7527	—	—	0.7528
	Liang[4]	0.9535	0.7535	0.9724	—	0.7015
Supervised methods	FC-CRF[18]	0.9454	0.7897	0.9684	—	0.7857
	HED[19]	0.9054	0.9563	0.9007	—	0.6400
	Line Operator [20]	0.9540	0.7680	0.9700	0.9700	—
	Cross-modality [21]	0.9527	0.7569	0.9816	0.9738	—
	DRIU[22]	0.9541	0.8261	0.9115	0.9541	0.6701
	U-Net	0.9585	0.6565	0.9800	0.9755	0.8142
	Our method	0.9663	0.8075	0.9814	0.9846	0.8203

in the real vessel pixels.Specificity indicates the percentage of correctly classified background pixels in the real background pixels. Accuracy represents the proportion of correctly classified blood vessels and background pixels in the whole image pixels. Additionally, TPR represents the percentage of classified vessel pixels in the whole vessel pixels. FPR represents the false classification of background pixels into the proportion of blood vessels in the real background pixels. In addition, F-measure represents the harmonic mean of the segmentation accuracy and recall rate.

The ROC curve is a method to measure the classification performance of the algorithm. The horizontal axis is the FPR, and the vertical axis is the TFR; the area under the ROC curve is the AUC value. The value is in between [0, 1]. The higher the AUC, the stronger is the forecast ability of the model. The ROC curve is shown in Fig. 9.

Table 1 and Table 2 respectively show the evaluation indices of the DRIVE and STARE datasets in different references.

Table 1 shows that the accuracy, sensitivity, specificity, AUC value and F-measure of the algorithm proposed in the paper for the DRIVE dataset are higher than those listed by the unsupervised learning methods, reflecting the advantages of supervised learning in vessel segmentation. The algorithm segmentation accuracy, AUC value and F-measure are higher than those listed by other supervised learning algorithms, showing that this algorithm can correctly classify more pixels of blood vessels. The sensitivity of the algorithm in this paper is 0.1488 and 0.0186 lower than that of the HED algorithm and DRIU algorithm, respectively, but the sizes of the segmented blood vessels are obviously thicker than the ground truth segmentation results, which contain significant noise information. The cross-modality algorithm presents 0.002 higher specificity (approximately negligible), but other lower evaluation indices than the algorithm in this paper.

As can be seen from Table 2, the accuracy, sensitivity, specificity and F-measure of the algorithm for the STARE

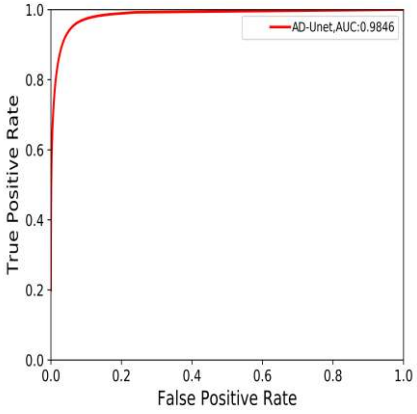

(a) ROC chart of the DRIVE dataset

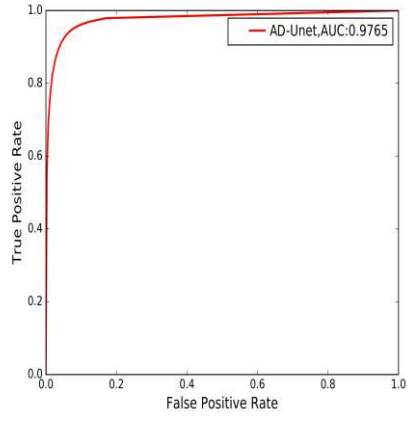

(b) ROC chart of the STARE dataset

FIGURE 9. ROC chart of the algorithm in this paper.

dataset are higher than those listed in the unsupervised learning methods, and the AUC value of the algorithm in this paper is 0.0115 lower than that in reference [16]; comparing evaluation indicators, all those of reference [16] are inferior to the algorithm in this paper, and the segmentation results in reference [16] show rupture of blood vessels. The accuracy

TABLE 2. Retinal vessel segmentation results of the STARE dataset.

Type	Method	Acc(%)	Sen(%)	Spe(%)	AUC	F-measure
Unsupervised methods	Mendonca[15]	0.9440	0.6990	0.9730	0.8360	—
	Soomro[16]	0.9410	0.7130	0.9680	0.9810	—
	Khan[17]	0.9670	0.7340	0.9670	—	—
	Wang[3]	0.9451	0.7686	—	—	0.7369
	Liang[4]	0.9503	0.7908	0.9629	—	0.6679
Supervised methods	FC-CRF[18]	0.9519	0.7680	0.9738	—	0.7644
	HED[19]	0.9378	0.9955	0.5555	—	0.6990
	Line Operator [20]	0.9570	0.7810	0.9770	0.9680	—
	Cross-modality [21]	0.9628	0.7726	0.9844	0.9879	—
	DRIU[22]	0.9499	0.6066	0.9956	0.9879	0.7385
	U-Net	0.9641	0.7361	0.9690	—	0.8273
	Our method	0.9684	0.8437	0.9762	0.9765	0.8419

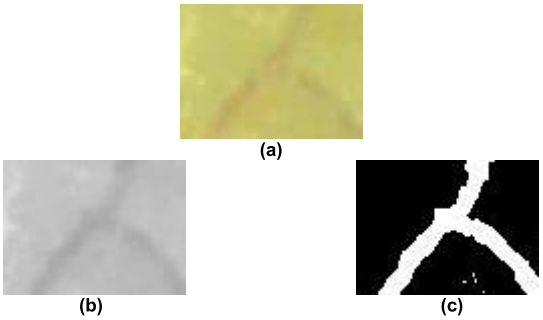

FIGURE 10. Image segmentation results of bulbar conjunctiva micro-vessels. (a) The original single-frame image, (b) A micro-vessel multi-frame fused images, (c) AD-UNet algorithm.

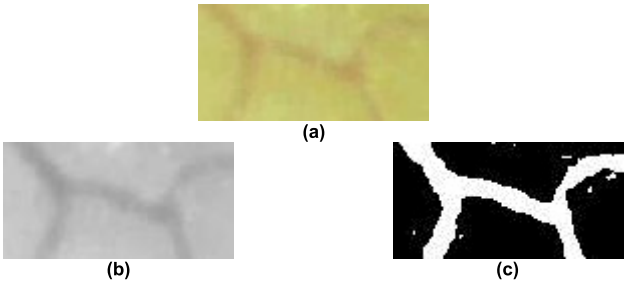

FIGURE 11. Image segmentation results of bulbar conjunctiva micro-vessels. (a) The original single-frame image,(b) A micro-vessel multi-frame fused images, (c) AD-UNet algorithm.

and F-measure of this algorithm are higher than those listed for other supervised learning methods. In terms of sensitivity, the value of the HED algorithm is 0.1518 higher than that of the algorithm in this paper. The HED algorithm can detect edge information with a small receptive field. Therefore, due to the influence of the network, the algorithm segments a large blood vessel size and sometimes produces fuzzy blood vessel segmentation results. As for the specificity, the value of the algorithm in this paper is 0.0008, 0.0082 and 0.0194 lower than the Line Operator algorithm, cross-modality algorithm and DRIU algorithm, respectively. However, the accuracy and F-measure of the algorithm in this paper are higher, and the segmentation results of the algorithm in this paper contain a small amount of noise information, which is not good for the segmentation results of tiny vessels at the ends of vessel branches. The AUC value of the algorithm in this paper is 0.0114 and 0.0114 lower than those of the cross-modality algorithm and DRIU algorithm, but 0.1034 higher than the DRIU algorithm with respect to the F-measure. The evaluation indices of the traditional U-Net measured for DRIVE and STARE are lower than those of the algorithm in this paper, indicating the necessity of adding the attention mechanism and dense connection. Therefore, it can be seen from the measurement indices in Table 1 and Table 2 that the performance of the algorithm in this paper is superior.

E. APPLICATION OF THE AD-UNET ALGORITHM FOR HUMAN BULBAR CONJUNCTIVAL MICRO-VESSEL SEGMENTATION

The algorithm in this paper is verified using the internationally recognized DRIVE and STARE datasets, and its advantages are proven. Therefore, this algorithm is applied in our project research to segment human bulbar conjunctival micro-vessels. Aiming at the problem that the original single-frame bulbar conjunctival micro-vessel images are all limited by red blood cells in the field of view, the pixel level fusion method is adopted to conduct multi-frame fusion processing on the collected 20-frame discontinuous micro-vessel green channel images. The multi-frame fused micro-vessels are segmented by the AD-UNet algorithm, and the segmentation results are shown in Fig. 10 and Fig. 11.

The experimental results show that the AD-UNet algorithm can obtain a more accurate micro-vessel contour, and more

effectively solve the problem of unsatisfactory vessel segmentation caused by blurry target edges and low contrast.

IV. CONCLUSION

Retinal vessel segmentation plays a significant role in assisting doctors in treating fundus diseases. In view of the low contrast between retinal blood vessels and the background, complex structural information and blurred boundaries between blood vessels and tissues, AD-UNet is proposed in the paper to segment retinal vessel images. It introduces the attention mechanism and DenseNet into U-Net, improves the utilization rate of feature information of the model and reduces the complexity of network learning parameters. Moreover, it locates the fundus contour areas more accurately by introducing the attention mechanism and better improves the segmentation accuracy. Experimental results demonstrate the superiority of the present algorithm to other supervised and unsupervised learning algorithms. Besides, the application of AD-UNet algorithm to the project of human bulbar conjunctiva microvessel segmentation in this paper is capable of deriving rather accurate segmentation results. However, our method is still needed to be improved. For example, in terms of unclear blood vessel edges and tissue boundaries in the image, unsmooth edges appear in the segmentation results for the vessel areas. Hence, there remains room for further improvement regarding the development of our method in the future.

REFERENCES

[1] G. B. Kande, T. S. Savithri, and P. V. Subbaiah, "Retinal vessel segmentation using histogram matching," in *Proc. IEEE Asia Pacific Conf. Circuits Syst.*, Macao, China, Nov./Dec. 2008, pp. 129–132.
[2] M. U. Akram, A. Atzaz, S. F. Aneeque, and S. A. Khan, "Blood vessel enhancement and segmentation using wavelet transform," in *Proc. Int. Conf. Digit. Image Process.*, Mar. 2009, pp. 34–38.
[3] X. H. Wang, Y. Q. Zhao, M. Liao, and B. Z. Zou, "Automatic segmentation for retinal vessel based on multi-scale 2D Gabor wavelet," *Acta Automatica Sinica*, vol. 41, no. 5, pp. 970–980, 2015.
[4] L. M. Liang, C. L. Huang, W. Shi, J. Wu, H. J. Jiang, and X. J. Chen, "Retinal vessel segmentation using level set combined with shape priori," *Chin. J. Comput.*, vol. 41, no. 7, pp. 1678–1692, 2018.
[5] A. Oliveira, S. Pereira, and C. A. Silva, "Retinal vessel segmentation based on fully convolutional neural networks," *Expert Syst. Appl.*, vol. 112, pp. 229–242, Dec. 2018.
[6] D. Marin, A. Aquino, M. E. Gegundez-Arias, and J. Bravo, "A new supervised method for blood vessel segmentation in retinal images by using gray-level and moment invariants-based features," *IEEE Trans. Med. Imag.*, vol. 30, no. 1, pp. 146–158, Jan. 2011.
[7] P. Liskowski and K. Krawiec, "Segmenting retinal blood vessels with deep neural networks," *IEEE Trans. Med. Imag.*, vol. 35, no. 11, pp. 2369–2380, Nov. 2016.
[8] Y. Jiang, N. Tan, T. Peng, and H. Zhang, "Retinal vessels segmentation based on dilated multi-scale convolutional neural network," *IEEE Access*, vol. 7, pp. 76342–76352, 2019.
[9] H. Fu, Y. Xu, D. W. K. Wong, and J. Liu, "Retinal vessel segmentation via deep learning network and fully-connected conditional random fields," in *Proc. IEEE 13th Int. Symp. Biomed. Imag. (ISBI)*, Apr. 2016, pp. 698–701.
[10] G. Huang, Z. Liu, L. van der Maaten, and K. Q. Weinberger, "Densely connected convolutional networks," in *Proc. IEEE Conf. Comput. Vis. Pattern Recognit. (CVPR)*, Jul. 2017, pp. 2261–2269.
[11] H. Zhou, Y. Zhang, L. Yang, Q. Liu, K. Yan, and Y. Du, "Short-term photovoltaic power forecasting based on long short term memory neural network and attention mechanism," *IEEE Access*, vol. 7, pp. 78063–78074, 2019.
[12] D. Bahdanau, K. Cho, and Y. Bengio, "Neural machine translation by jointly learning to align and translate," in *Proc. ICLR*, May 2016, pp. 1–15.
[13] J. Staal, M. D. Abramoff, M. Niemeijer, M. A. Viergever, and B. van Ginneken, "Ridge-based vessel segmentation in color images of the retina," *IEEE Trans. Med. Imag.*, vol. 23, no. 4, pp. 501–509, Apr. 2004.
[14] A. D. Hoover, V. Kouznetsova, and M. Goldbaum, "Locating blood vessels in retinal images by piecewise threshold probing of a matched filter response," *IEEE Trans. Med. Imag.*, vol. 19, no. 3, pp. 203–210, Mar. 2000.
[15] A. M. Mendonca and A. Campilho, "Segmentation of retinal blood vessels by combining the detection of centerlines and morphological reconstruction," *IEEE Trans. Med. Imag.*, vol. 25, no. 9, pp. 1200–1213, Sep. 2006.
[16] T. A. Soomro, M. A. U. Khan, J. Gao, T. M. Khan, and M. Paul, "Contrast normalization steps for increased sensitivity of a retinal image segmentation method," *J. Signal Image Video Process.*, vol. 11, no. 8, pp. 1509–1517, 2017.
[17] M. A. U. Khan, T. A. Soomro, T. M. Khan, D. G. Bailey, J. Gao, and N. Mir, "Automatic retinal vessel extraction algorithm based on contrast-sensitive schemes," in *Proc. Int. Conf. Image Vis. Comput. New Zealand (IVCNZ)*, Palmerston North, New Zealand, Nov. 2016, pp. 1–5.
[18] J. I. Orlando, E. Prokofyeva, and M. B. Blaschko, "A discriminatively trained fully connected conditional random field model for blood vessel segmentation in fundus images," *IEEE Trans. Biomed. Eng.*, vol. 64, no. 1, pp. 16–27, Jan. 2017.
[19] S. Xie and Z. Tu, "Holistically-nested edge detection," *Int. J. Comput. Vis.*, vol. 125, nos. 1–3, pp. 3–18, Dec. 2017.
[20] T. Na, J. Xie, Y. Zhao, Y. Zhao, Y. Liu, Y. Wang, and J. Liu, "Retinal vascular segmentation using superpixel-based line operator and its application to vascular topology estimation," *Med. Phys.*, vol. 45, no. 7, pp. 3132–3146, Jul. 2018.
[21] Q. Li, B. Feng, L. Xie, P. Liang, H. Zhang, and T. Wang, "A cross-modality learning approach for vessel segmentation in retinal images," *IEEE Trans. Med. Imag.*, vol. 35, no. 1, pp. 109–118, Jan. 2016.
[22] K. Maninis, J. Pont-Tuset, P. Arbelaez, and L. V. Gool, "Deep retinal image understanding," in *Proc. MICCAI*, 2016, pp. 140–148.
[23] J. Son, S. J. Park, and K.-H. Jung, "Retinal vessel segmentation in fundoscopic images with generative adversarial networks," 2017, *arXiv:1706.09318*. [Online]. Available: https://arxiv.org/abs/1706.09318
[24] D. A. Dharmawan, D. Li, B. P. Ng, and S. Rahardja, "A new hybrid algorithm for retinal vessels segmentation on fundus images," *IEEE Access*, vol. 7, pp. 41885–41896, Mar. 2019.
[25] X. Ren, Y. Zheng, Y. Zhao, C. Luo, H. Wang, J. Lian, and Y. He, "Drusen segmentation from retinal images via supervised feature learning," *IEEE Access*, vol. 6, pp. 2952–2961, 2017.
[26] P. Xiuqin, Q. Zhang, H. Zhang, and S. Li, "A fundus retinal vessels segmentation scheme based on the improved deep learning U-Net model," *IEEE Access*, vol. 7, pp. 122634–122643, 2019. doi: 10.1109/ACCESS.2019.2935138.
[27] C. Wang, "Dense U-net based on patch-based learning for retinal vessel segmentation," in *Entropy*, vol. 21, no. 2, p. 168, Feb. 2019.
[28] X. Li, Y. Hong, D. Kong, and X. Zhang, "Automatic segmentation of levator hiatus from ultrasound images using U-net with dense connections," *Phys. Med. Biol.*, vol. 64, no. 7, Apr. 2019, Art. no. 075015.
[29] M. Z. Alom, M. Hasan, C. Yakopcic, T. M. Taha, and V. K. Asari, "Recurrent residual convolutional neural network based on U-net (R2U-Net) for medical image segmentation," *J. Med. Imag.*, vol. 6, no. 1, pp. 1–12, Feb. 2018. [Online]. Available: https://arxiv.org/abs/1802.06955

ZHONGMING LUO held a visiteur position with the École de technologie supérieure, Université du Québec, Canada, in 1997. He was a Visiting Researcher with the Tokyo Institute of Technology, Japan, from 2006 to 2007. He is currently a Professor of measurement and control technology and communication engineering with the Harbin University of Science and Technology, China.

Dr. Luo is the Standing Director of the Electromagnetic Measurement and Information Processing Instrument Branch of China Instrument and Control Society (ECIS) and a Committee Member of the National Standardization Committee for Electrical Measuring Instruments (SAC/TC104).

YU ZHANG received the bachelor's degree in communication engineering form the Northeast Agricultural University Chengdong College, in 2016. He is currently pursuing the M.E. degree in Harbin University of Science and Technology, Heilongjiang, China. His research interests include medical image processing and deep learning algorithm.

LEI ZHOU received the B.E. degree in Internet of Things from the Harbin university of Science and Technology, Harbin, China, where he is currently pursuing the master's degree in instrument engineering. He was been a Freshman with the School of Measurement and Control Technology & Communication Engineering, since 2018. His research interests include digital system design and IC design.

BINGE ZHANG has taught at Heilongjiang Institute of Construction Technology, China, for 37 years, where he is currently an Associate Professor.

JIANAN LUO is currently pursuing the master's degree from the School of Measurement and Control Technology and Communication Engineering, Harbin University of Science and Technology, China, where she has been a member with the Image Processing of Biological Information Laboratory, since 2018. Her research interests include the deep learning and image segmentation algorithm.

HAIBIN WU is currently a Professor of measurement and control technology and communication engineering with the Harbin University of Science and Technology, China. His research interests include 3D vision measurement, machine vision, and virtual reality.

Dr. Wu is the Director of the Precision Machinery Branch of China Instrument Association.